THE JOURNAL OF BIOLOGICAL CHEMISTRY VOL. 291, NO. 33, pp. 17133–17142, August 12, 2016
© 2016 by The American Society for Biochemistry and Molecular Biology, Inc. Published in the U.S.A.

Crystal Structure of Human Leukocyte Cell-derived Chemotaxin 2 (LECT2) Reveals a Mechanistic Basis of Functional Evolution in a Mammalian Protein with an M23 Metalloendopeptidase Fold*

Received for publication, February 9, 2016, and in revised form, June 11, 2016 Published, JBC Papers in Press, June 22, 2016, DOI 10.1074/jbc.M116.720375

Hai Zheng[‡], Takuya Miyakawa[‡], Yoriko Sawano[‡§], Atsuko Asano[‡], Akinori Okumura[¶], Satoshi Yamagoe[‖], and Masaru Tanokura[‡1]

From the [‡]Department of Applied Biological Chemistry, Graduate School of Agricultural and Life Sciences, The University of Tokyo, 1-1-1 Yayoi, Bunkyo-ku, Tokyo 113-8657, Japan, [§]Department of Chemistry, College of Liberal Arts and Sciences, Tokyo Medical and Dental University, 2-8-30 Kounodai, Ichikawa-shi, Chiba 272-0827, Japan, [¶]Department of Diabetic Complications, Diabetes Research Center, Research Institute, National Center for Global Health and Medicine, 1-21-1 Toyama, Shinjuku-ku, Tokyo 162-8655, Japan, and [‖]Department of Chemotherapy and Mycoses, National Institute of Infectious Diseases, 1-23-1 Toyama, Shinjuku-ku, Tokyo 162-8640, Japan

Human leukocyte cell-derived chemotaxin 2 (LECT2), which is predominantly expressed in the liver, is a multifunctional protein. LECT2 is becoming a potential therapeutic target for several diseases of worldwide concern such as rheumatoid arthritis, hepatocellular carcinoma, and obesity. Here, we present the crystal structure of LECT2, the first mammalian protein whose structure contains an M23 metalloendopeptidase fold. The LECT2 structure adopts a conserved Zn(II) coordination configuration but lacks a proposed catalytic histidine residue, and its potential substrate-binding groove is blocked in the vicinity of the Zn(II)-binding site by an additional intrachain loop at the N terminus. Consistent with these structural features, LECT2 was found to be catalytically inactive as a metalloendopeptidase against various types of peptide sequences, including pentaglycine. In addition, a surface plasmon resonance analysis demonstrated that LECT2 bound to the c-Met receptor with micromolar affinity. These results indicate that LECT2 likely plays its critical roles by acting as a ligand for the corresponding protein receptors rather than as an enzymatically active peptidase. The intrachain loop together with the pseudo-active site groove in LECT2 structure may be specific for interactions between LECT2 and receptors. Our study reveals a mechanistic basis for the functional evolution of a mammalian protein with an M23 metalloendopeptidase fold and potentially broadens the implications for the biological importance of noncatalytic peptidases in the M23 family.

Leukocyte cell-derived chemotaxin 2 (LECT2)[2] is a secretory protein originally identified as a chemotactic factor for neutrophils (1). LECT2 is predominantly expressed in the liver and is a direct target gene of Wnt/β-catenin signaling (2–6). Accumulating evidence shows that mammalian LECT2 is a multifunctional protein that is closely associated with several diseases of worldwide concern, including hepatitis (7), rheumatoid arthritis (8–10), hepatocellular carcinoma (HCC) (11, 12), obesity (13, 14), and renal and hepatic amyloidosis (15–17). It has been reported that concanavalin A-induced hepatitis and collagen antibody-induced arthritis were suppressed by LECT2 (7, 8). In addition, LECT2 expression inhibited the migration and invasion of human HCC cells *in vitro* and was negatively correlated with vascular invasion and tumor recurrence in HCC patients (11). In contrast, serum LECT2 levels were positively correlated with the severity of obesity and fatty liver in humans, and overproduction of LECT2 caused the development of obesity-associated insulin resistance (13, 14). These findings suggest that LECT2 may be a candidate prognostic marker and a potential therapeutic target for these diseases. Despite the importance of LECT2 functions, the underlying mechanisms remain largely unclear.

The mature human LECT2 is a basic protein consisting of 133 amino acids. Sequence similarity searches using BLAST have shown that LECT2 has a putative peptidase-M23 (PF01551) domain located between amino acids 33 and 129 (18, 19). M23 family members are typically zinc-dependent metalloendopeptidases that cleave the peptide cross-bridges in the peptidoglycans in cell walls and have a specificity that targets glycylglycine peptide bonds (20–23). They are divided into two subclasses based on sequence homology: the M23A family, which includes the β-lytic endopeptidase from *Lysobacter enzymogenes* and LasA from *Pseudomonas aeruginosa*, and the M23B family, which consists of the majority of the family members, including LytM from *Staphylococcus aureus* (22, 24). The M23A endopeptidases possess broader substrate specificities than those of the M23B endopeptidases (22, 24). Proteins of the M23 family are distinguished by conserved Zn(II)-binding res-

* This work was supported by the Targeted Proteins Research Program of the Ministry of Education, Culture, Sports, Science and Technology, Japan (MEXT); by the Platform for Drug Discovery, Informatics, and Structural Life Science from MEXT; and by a grant-in-aid for scientific research (S) from the Japan Society for the Promotion of Science. The authors declare that they have no conflicts of interest with the contents of this article.

The atomic coordinates and structure factors (code 5B0H) have been deposited in the Protein Data Bank (http://wwpdb.org/).

[1] To whom correspondence should be addressed. Tel.: 81-3-5841-5165; Fax: 81-3-5841-8023; E-mail: amtanok@mail.ecc.u-tokyo.ac.jp.

[2] The abbreviations used are: LECT2, leukocyte cell-derived chemotaxin 2; HCC, hepatocellular carcinoma; IC, intrachain; c-Met, c-mesenchymal epithelial transition factor; ECD, extracellular domain; K_D, dissociation constant; SeMet, selenomethionine; r.m.s.d., root mean square deviation.

idues that occur in the HX_nD (H*XXX*D for M23B) and H*X*H motifs (24–28). These residues allow Zn(II) to polarize the substrate carbonyl oxygen to increase the susceptibility to nucleophilic attack. An active site histidine that does not coordinate Zn(II) abstracts a proton from Zn(II)-bound water and donates it to the departing amide nitrogen of the substrate, resulting in cleavage of the peptide bond (24, 29).

The known M23 family members are all present in bacteriophages and bacteria (19). The peptidoglycan hydrolase activities are required for their physiological roles, including cell division, cell elongation, and bacteriophage infection (29–31). However, human LECT2 is the sole mammalian protein in the M23 family. Although the sequence of LECT2 contains conserved motifs (H*XXX*D and H*X*H), it is unclear whether LECT2 has a metalloendopeptidase activity. Moreover, there is no evidence that the functions of LECT2 require enzymatic catalysis. Thus, it remains unclear whether a peptidase activity is required for the roles of LECT2 in various diseases. Most recently, it was reported that LECT2 can bind to the receptor tyrosine kinase human c-mesenchymal epithelial transition factor (c-Met). This binding is antagonistic to the c-Met receptor activation, and LECT2 acts as a tumor suppressor in HCC (32). This finding suggests an alternative function in which LECT2 is involved in protein-protein interaction.

Here, we present the crystal structure of human LECT2 at 1.94-Å resolution. This is the first mammalian protein whose structure has been confirmed to contain an M23 metalloendopeptidase fold. The LECT2 structure contains the conserved Zn(II) coordination geometry that uses the H*XXX*D and H*X*H motifs but lacks a proposed catalytic histidine residue (residue 86 is a Tyr instead of a His). Furthermore, a unique N-terminal intrachain (IC) loop blocks the potential substrate-binding groove in the vicinity of the Zn(II)-binding site, which may hinder the suitable positioning of the substrate for hydrolysis. Our proteolytic assays show that LECT2 lacks endopeptidase activity against various peptide sequences, including pentaglycine, which is consistent with its structural features. In addition, our study reveals the possible receptor-binding sites in the LECT2 structure and provides a better understanding of the functional evolution of a mammalian protein with an M23 metalloendopeptidase fold.

Results

Overall Structure of LECT2—The crystal structure of LECT2 was determined at 1.94-Å resolution. There were two molecules in the asymmetric unit, and each chain was composed of residues 1–133 (numbering is given for the mature LECT2). The root mean square deviation (r.m.s.d.) value was 0.34 Å for the aligned C^{α} atoms between two chains in an asymmetric unit, which shows that there was no significant structural difference between the chains. Because the electron density in chain B was clearer than that of chain A, the following results for chain B are described. The LECT2 structure possesses a large groove with a Zn(II) at the bottom (Fig. 1). The floor of this groove is formed by a central, six-stranded antiparallel β-sheet (β1, β9, β5, β4, β3, and β7), and its walls consist of four loops: loop 1 (Gly^{25}–Gly^{37}, located at the N terminus), loop 2 (Glu^{60}–Asn^{71}, which connects β3 and β4), loop 3 (Leu^{106}–Ser^{117}, which connects β8 and β9), and loop 4 (Cys^{124}–Pro^{129}, located at the C terminus). Loops 3 and 4 formed a partial α-helix (α1) and a 3_{10}-helix (η1), respectively. In addition to the central β-sheet, there is a second, much smaller three-strand β-sheet (β2, β8, and β6), which runs parallel to the central β-sheet and is positioned on the lower face of the central β-sheet. In addition, the structure includes three disulfide bonds, Cys^{7}-Cys^{42}, Cys^{18}-Cys^{23}, and Cys^{81}-Cys^{124}, which is consistent with previous assignments of disulfide linkages using mass spectrometry (18).

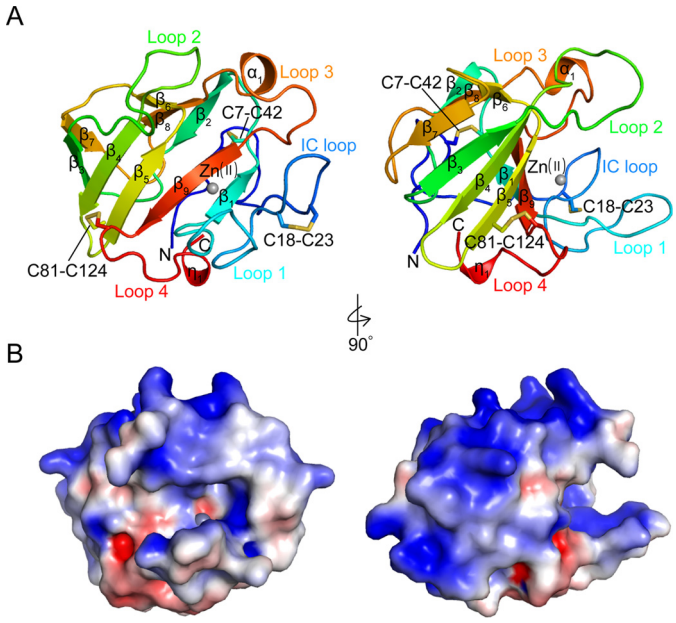

FIGURE 1. **Overall structure of LECT2.** *A*, ribbon diagram of the LECT2 structure. The color coding ranges from *blue* at the N terminus to *red* at the C terminus. The Zn(II) is shown as a *gray sphere*, and the disulfide bonds are shown as *yellow sticks*. *B*, surface representation of LECT2 colored according to the electrostatic potential. The colors change continuously from a negative potential of $-3\ k_BT/q$ (where k_B is the Boltzmann constant, T is the temperature, and q is the magnitude of the charge on an electron) (*red*) to a positive potential of $3\ k_BT/q$ (*blue*).

A database search using the Dali server showed the close structural similarity of LECT2 to the M23 metalloendopeptidases, including the catalytic domains of the M23B endopeptidases LytM (Protein Data Bank code 2B13; Z score, 12.6; sequence identity, 22%; r.m.s.d. for 111 C^{α} atoms, 2.5 Å) and lysostaphin (Protein Data Bank code 4QP5; Z score, 12.5; sequence identity, 19%; r.m.s.d. for 109 C^{α} atoms, 2.2 Å) and the M23A endopeptidase LasA (Protein Data Bank code 3IT7; Z score, 9.0; sequence identity, 16%; r.m.s.d. for 109 C^{α} atoms, 3.4 Å) (Fig. 2*A*) (24, 26, 28). These three classical M23 family members all specifically target the pentaglycine cross-links present in *S. aureus* peptidoglycan. Furthermore, LasA can cleave a wider range of glycine-rich peptides with aromatic or branched amino acids at the P1′ position such as Pro-Gly-Gly ↓ Tyr-Gly and Leu-Gly-Gly ↓ Ala-Gly (↓ denotes the cleavage site) (24, 26, 28, 33). A superimposition of the structures of LECT2 and LytM revealed that the central β-sheet of LECT2 was similar to that of LytM, which consists of six antiparallel β-strands with a conserved topology, but loops 1–4 in the two structures showed significant differences in the lengths and conformations (Fig. 2*B*). A similar variability of loop regions is also found

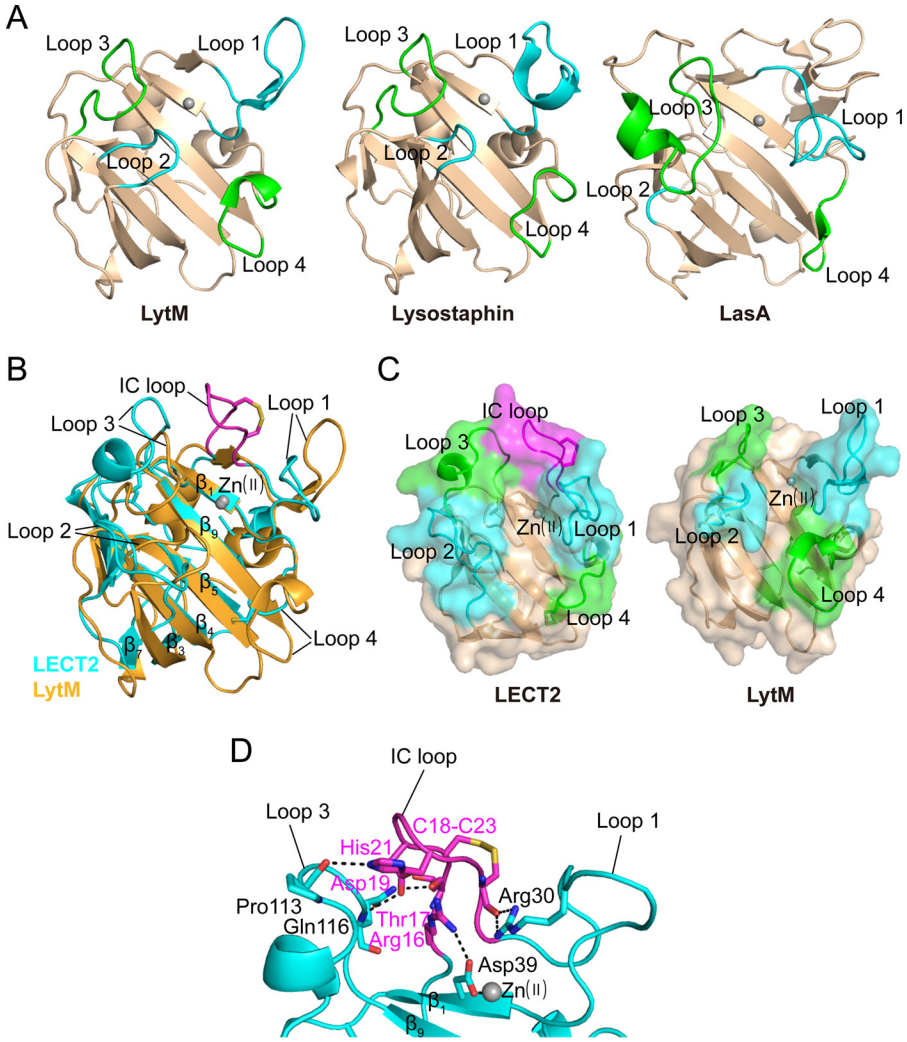

FIGURE 2. **Structural comparison between LECT2 and other M23 metalloendopeptidases.** *A*, structures of LytM, lysostaphin, and LasA. Loops 1 and 2 are colored *cyan*, and loops 3 and 4 are colored *green*. The Zn(II) is shown as a *gray sphere*. *B*, superimposed structures of LECT2 (*cyan*) and LytM (*orange*). The disulfide bonds of LECT2 are shown as *yellow sticks*. The IC loop is highlighted in *magenta*. *C*, surface comparison of LECT2 (*left*) and LytM (*right*). The color scheme for loops 1–4 is described above. The IC loop of LECT2 is shown as a *magenta surface* between loops 1 and 3. *D*, interactions of the IC loop with loops 1 and 3. The LECT2 structure is colored *cyan*, and the IC loop is highlighted in *magenta*. The interacting residues are shown as *stick* models with the nitrogen, oxygen, and sulfur atoms colored *blue*, *red*, and *yellow*, respectively. The hydrogen bonds are shown as *black dashed lines*.

in other structural homologs (Fig. 2*A*). This variability likely reflects the different substrate specificities as indicated by the broader specificity of LasA than that of LytM or lysostaphin (24). Additionally, a notable difference in the LECT2 structure is an insertion of a protruding IC loop region formed by the Cys^{18}-Cys^{23} disulfide bond, which immediately precedes loop 1 (Fig. 2*B*). This N-terminal IC loop lies at one end of the groove of LECT2 and is stabilized by several interactions (Figs. 2, *C* and *D*). First, there is a hydrogen bond between the side chains of Arg^{16} on the IC loop and Asp^{39} on strand $\beta1$. Second, the main chain of Thr^{17} on the IC loop forms a hydrogen bond with the side chain of Gln^{116} on loop 3, and the side chain of Asp^{19} on the IC loop makes a hydrogen bond with the main chain of Gln^{116} on loop 3. Third, the side chain of His^{21} forms a hydrogen bond with the main chain of Pro^{113} on loop 3. Fourth, the main chain of Cys^{23} on the IC loop makes two hydrogen bonds with the side chain of Arg^{30} on loop 1.

Zn(II) Coordination Geometry—In the LECT2 structure, Zn(II) is coordinated by His^{35} (Zn(II)–$N^{\varepsilon2}$, 2.02 Å) and Asp^{39} (Zn(II)–$O^{\delta1}$, 2.00 Å) of the H*XXX*D motif, His^{120} (Zn(II)–$N^{\delta1}$, 2.09 Å) (the second histidine of the H*X*H motif), and a water molecule (2.77 Å) (Fig. 3*A*). The distance between Zn(II) and the water molecule (2.77 Å) is longer than the typical Zn(II)-ligand distance. Therefore, there may also be other Zn(II)-binding water molecules, but they are not defined in our structure due to the poor electron density. The four Zn(II) ligands as described above are fixed in space by hydrogen bonds to other amino acid residues (Fig. 3*A*). Because the $N^{\varepsilon2}$ of His^{35} directly contacts the Zn(II), the $N^{\delta1}$ is protonated and donates a hydrogen bond to the backbone carbonyl oxygen of Gln^{25} (2.83 Å). This pattern of interaction is known as an elec-His-Zn motif (34) and is believed to make the histidine imidazole ring more basic. Thus, His^{35} acts as a stronger ligand to the Zn(II). The $O^{\delta2}$ of Asp^{39} accepts a hydrogen bond from the guanidino nitrogen of Arg^{16} (2.88 Å) to stabilize the IC loop as mentioned above. The $N^{\varepsilon2}$ of His^{120} donates a hydrogen bond to the $O^{\varepsilon2}$ of Glu^{122} (2.66 Å) to form the other elec-His-Zn motif. In addition, the water molecule donates hydrogen bonds to the $N^{\varepsilon2}$ of

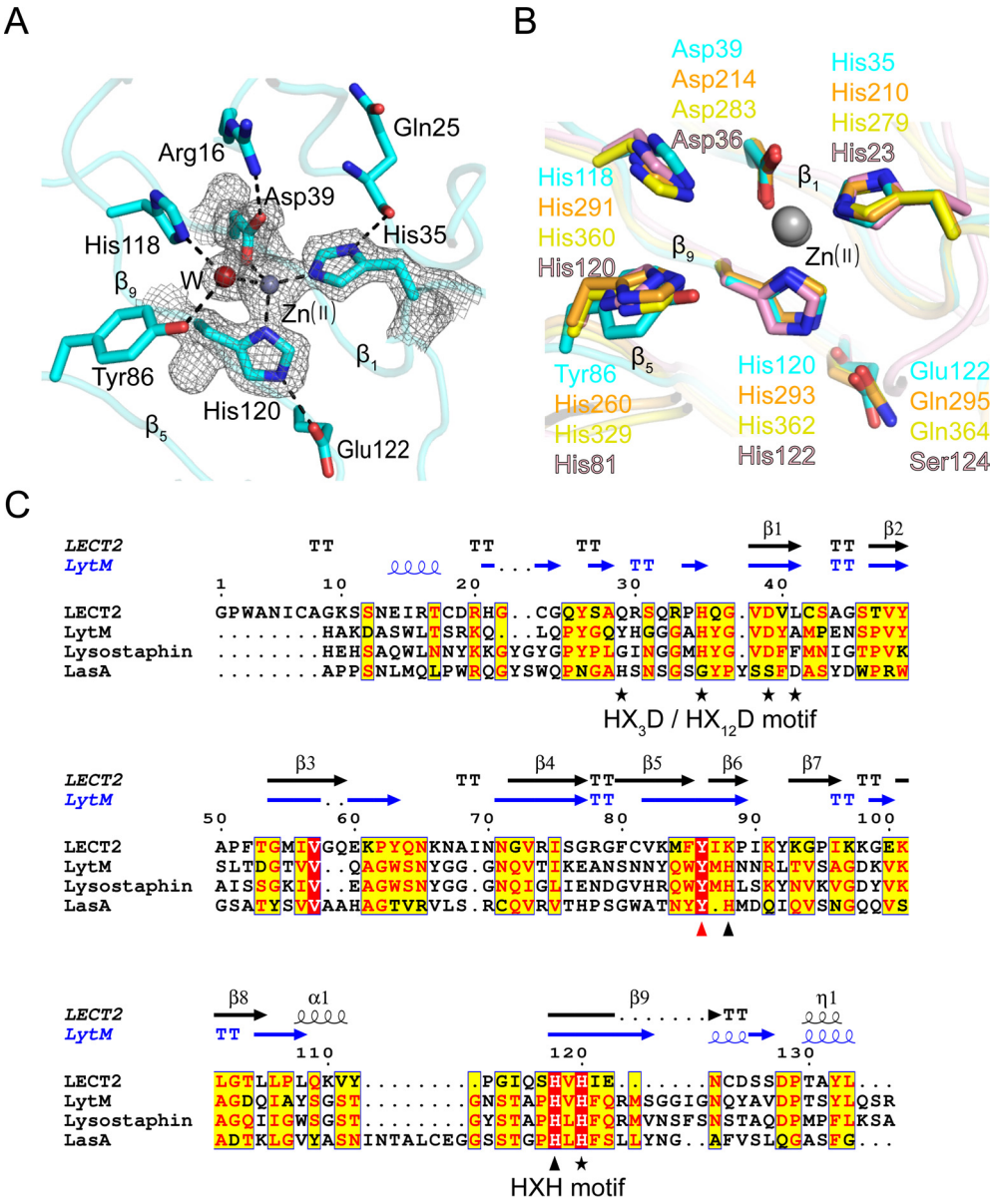

FIGURE 3. **Zn(II)-binding site of LECT2 and comparison with other M23 metalloendopeptidases.** *A*, Zn(II)-binding site of LECT2. Key residues are shown as *stick* models. Zn(II) and a water molecule are represented as *gray* and *red spheres*, respectively. The $2F_o - F_c$ electron density map for the Zn(II) and Zn(II) ligands is shown as a *gray mesh* (contoured at 1σ). The hydrogen bonding and Zn(II)-ligand interactions are shown as *black dashed lines*. *B*, superimposition of the Zn(II)-binding sites of LECT2, LytM, lysostaphin, and LasA. The conserved residues are shown as *stick* models with those of LECT2 in *cyan*, of LytM in *orange*, of lysostaphin in *yellow*, and of LasA in *pink*. *C*, LECT2 sequence alignment with other M23 metalloendopeptidases. The residue numbering is for LECT2. The secondary structure elements are indicated by *helices* (α- or 3_{10}-helices), *arrows* (β-strands), and *TT letters* (β-turns) above the alignment sequences. The *black stars* indicate the important residues for Zn(II) binding. The *black triangles* show two proposed catalytic histidines for LytM, lysostaphin, and LasA, and a *red triangle* represents the tyrosine residue of LECT2 that replaces the catalytic histidine.

His^{118} (2.86 Å), which is the first histidine residue of the H*X*H motif, and the hydroxy oxygen of Tyr^{86} (2.95 Å). The superimposition shows that the Zn(II)-binding site of LECT2 closely resembles those of three other structural homologs (Fig. 3*B*). The three Zn(II) amino acid ligands as well as one of the two residues involved in acid-base catalysis (His^{118} for LECT2) have almost the same spatial location and orientation in the four structures. However, the position of other proposed catalytic histidine residue, for example His^{260} of LytM, is replaced by a tyrosine residue (Tyr^{86}) in LECT2, although this conserved histidine and LECT2 Tyr^{86} have different sequence alignments (Fig. 3, *B* and *C*). Such a variation has not been previously observed in M23 metalloendopeptidases.

Absence of M23 Metalloendopeptidase Activity in LECT2—LECT2 contains a unique IC loop and lacks one of the two proposed catalytic histidine residues (Tyr^{86} replaces the conserved His). The two catalytic histidines present unprotonated N$^{\delta 2}$ atoms toward the Zn(II)-binding water molecule and are proposed to play alternate roles, either activating the water molecule as a proton acceptor to perform the nucleophilic attack upon the substrate carbonyl carbon or stabilizing the oxyanion intermediate (24, 29). To clarify whether LECT2 functions as an M23 metalloendopeptidase and whether the lack of the conserved histidine residue causes the loss of the M23 metalloendopeptidase activity, we investigated hydrolysis of the typical pentaglycine substrate by both the wild-type

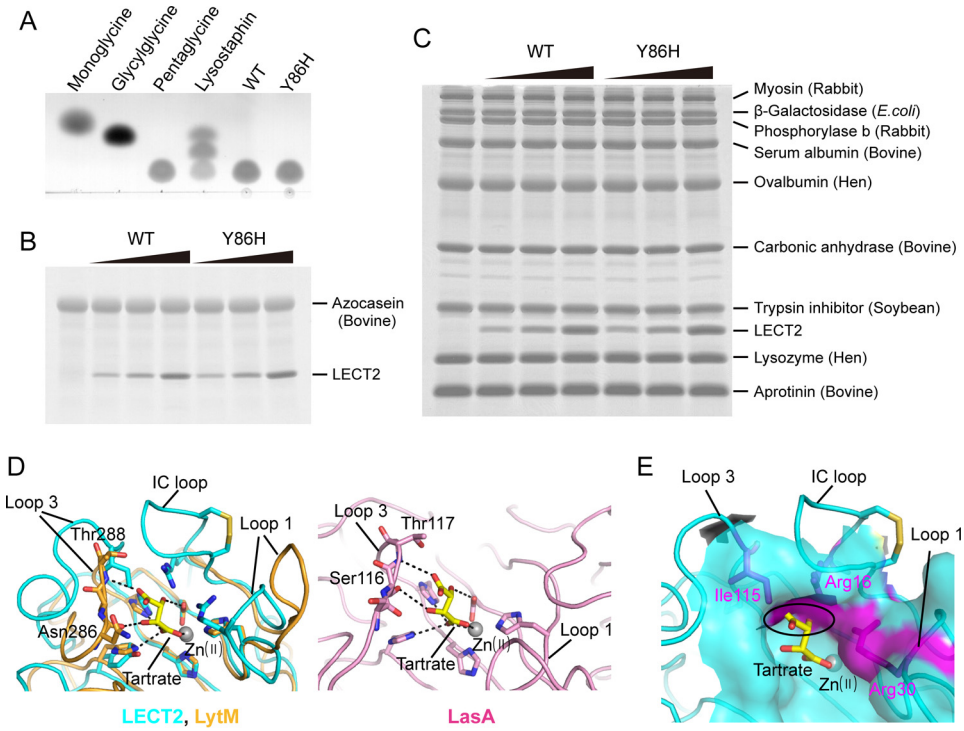

FIGURE 4. **Absence of M23 metalloendopeptidase activity in LECT2.** *A*, determination of glycylglycine endopeptidase activity using the TLC method. Pentaglycine was used as the substrate and incubated with lysostaphin (positive control) and the wild-type (WT) or Y86H mutant (Y86H) of LECT2 at 37 °C for 24 h. *B*, endopeptidase assay against azocasein as a substrate. Azocasein was incubated with various concentrations (1, 2, and 5 μM) of the LECT2 WT or Y86H mutant protein at 37 °C for 24 h. *C*, endopeptidase assay against nine proteins (myosin, β-galactosidase, phosphorylase *b*, serum albumin, ovalbumin, carbonic anhydrase, trypsin inhibitor, lysozyme, and aprotinin) as substrates. These proteins were incubated with the various concentrations (1, 2, and 5 μM) of the LECT2 WT or Y86H mutant protein at 37 °C for 24 h. *D*, interactions of the tartrate molecule with the active sites of M23 metalloendopeptidases. *Left*, the tartrate binding in the LytM active site (*orange*) and superimposition onto the putative active site of LECT2 (*cyan*). *Right*, the tartrate binding in the LasA active site (*pink*). The interactions made by bound tartrate (*yellow*) are represented by *dashed lines*. The residues on loop 3 that interact with the tartrate molecule are labeled. *E*, surface representation of LECT2 showing the steric hindrance with the tartrate molecule. The three residues Ile^{115}, Arg^{16}, and Arg^{30} in the vicinity of Zn(II) are colored in *magenta* and shown as *stick* models. The tartrate molecule from LytM is shown as *yellow sticks* with the oxygen atoms colored *red*.

LECT2 and the Y86H mutant using the thin-layer chromatography (TLC) method (Fig. 4*A*). Lysostaphin was chosen as a positive control because it is commercially available. Lysostaphin cleaved pentaglycine into di- and triglycine. In contrast, LECT2 did not cause cleavage of pentaglycine, although Tyr^{86} is likely to have the same ability as the histidine residue based on the chemical properties of the aromatic hydroxy group. Furthermore, the Y86H mutant was also not able to cleave the pentaglycine substrate.

To evaluate further endopeptidase activities of LECT2 and its Y86H mutant, we used various types of proteins (azocasein, myosin, β-galactosidase, phosphorylase *b*, serum albumin, ovalbumin, carbonic anhydrase, trypsin inhibitor, lysozyme, and aprotinin) as substrates in the proteolytic assays. With increasing concentrations of LECT2 from 1 to 5 μM, the azocasein bands on SDS-PAGE remained unchanged compared with the control sample that contained only azocasein (Fig. 4*B*). Similarly to the results for pentaglycine, the endopeptidase activity against azocasein could not be restored by the Y86H mutation. Furthermore, the band patterns of the other proteins were not changed by the reaction with LECT2 or its Y86H mutant (Fig. 4*C*). These results show that LECT2 has no endopeptidase activity against various types of peptide sequences.

We tried to explain the lack of LECT2 endopeptidase activity against pentaglycine and various other peptide sequences on the basis of the structural features of LECT2. In the structures of LytM and LasA, the binding patterns of tartrate molecules at the active sites are proposed to resemble those of the hydrolyzed products such as glycylglycine (24, 26). We therefore superimposed the structures of LECT2 and LytM to examine the tartrate binding in the groove of LECT2 (Fig. 4*D*, *left*). For LytM and LasA, the tartrate molecules make hydrogen bonds to Asn^{286} and Thr^{288} on loop 3 of LytM and to Ser^{116} and Thr^{117} on loop 3 of LasA. These results indicate that loop 3 is important for the proper positioning of substrates in the active site (Fig. 4*D*). In contrast, loop 3 of LECT2 projects away from the tartrate molecule (Fig. 4*D*, *left*). This loop conformation may be unfavorable for binding of substrates such as pentaglycine. More importantly, the tartrate molecule in the superimposed structures shows steric interference with Arg^{16} and Ile^{115} on the IC loop and loop 3 of LECT2 (Fig. 4*E*). The wall composed of the three residues Ile^{115}, Arg^{16}, and Arg^{30} makes the space in the vicinity of the LECT2 Zn(II)-binding site too narrow to accommodate the small tartrate molecule that is bound in the active site of LytM, clearly indicating that the groove of LECT2 may sterically hinder the binding of the amino acid, at least at the P2 site of a peptide substrate. For the M23 metalloendopeptidases, both sites P2 and P′2 in a short peptide (P3-P2-P1 ↓ P′1-P′2-P′3) must be occupied for hydrolysis to occur. This is most likely because the conformation

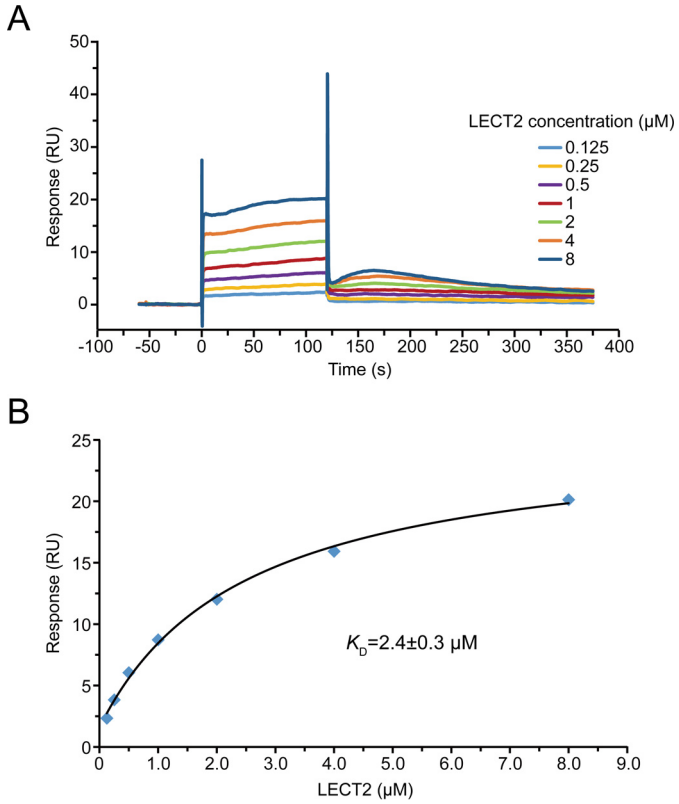

FIGURE 5. **Surface plasmon resonance analysis of 0.125–8 μM LECT2 binding to immobilized c-Met ECD.** *A*, sensorgrams showing an increase in response units (*RU*) as LECT2 in the mobile phase binds to c-Met ECD followed by a decrease as the complex dissociates. *B*, plot of the amplitude of the change in response units against the concentration of LECT2 from which a K_D value of 2.4 ± 0.3 μM was calculated.

of a peptide substrate is stabilized by a hydrogen bond between P1 and P4 residues (33). Conversely, this structure suggests that LECT2 could accept the substrate into the Zn(II)-binding site to exert exopeptidase activity because such activity does not require the P2 or P2′ site. However, no exopeptidase activity of LECT2 was observed when pentaglycine was used as a substrate (Fig. 4*A*).

Binding of LECT2 to c-Met Extracellular Domain (ECD)—Although LECT2 did not cause the cleavage of pentaglycine, LECT2 had the capacity for protein-protein interaction. The interaction between LECT2 and c-Met ECD has been demonstrated by coimmunoprecipitation experiments. The LECT2 binding caused an antagonistic effect on the c-Met receptor activation (32). In our study, the kinetic measurements of the interaction between these proteins were performed for the first time using surface plasmon resonance methods. Sensorgrams of the LECT2 binding to c-Met ECD were used to calculate the dissociation constant (K_D). The results showed that LECT2 bound to c-Met ECD with a K_D value of 2.4 ± 0.3 μM (Fig. 5). Normally, the c-Met signaling pathway is driven by its cognate ligand, hepatocyte growth factor (35). The β-chain of hepatocyte growth factor binds to c-Met ECD with a K_D of 90 nM (35), which is a higher affinity than that of LECT2 for c-Met ECD. However, these two ligands for c-Met do not interfere with each other (32). Thus, LECT2 is a noncompetitive c-Met antagonist.

Discussion

The LECT2 structure possesses an M23 metalloendopeptidase fold and a conserved Zn(II) coordination using the metal-chelating motifs H*XXX*D and H*X*H but lacks a proposed catalytic histidine residue (Tyr^{86} replaces the conserved His) and contains a unique N-terminal IC loop. A structural comparison of LECT2 with other M23 members demonstrated that the lack of endopeptidase activity for LECT2 could be ascribed to its distinct structural features. The tartrate-bound structures of LytM and LasA (Fig. 4*B*) and a proposed complex model of LasA with a pentapeptide substrate (Gly-Gly-Phe-Gly-Gly) showed that their central groove is the substrate binding site, and loop 3, which shows a significant sequence conservation, plays a critical role in substrate specificity, in particular by restricting the P1 site to glycine. However, for LECT2, the residues on loop 3 are not conserved (Fig. 3*C*). Loops 1 and 3 interact with the unique IC loop, forming an additional wall surrounding the Zn(II)-binding site at one end of the groove (Fig. 4*E*). On the basis of these structural differences, the substrate may not be bound to LECT2 in a manner suitable for hydrolysis.

The receptor tyrosine kinase c-Met has been identified as a LECT2-binding protein, and LECT2 binding suppresses the c-Met phosphorylation through the recruitment of protein-tyrosine phosphatase 1B. This results in the dissociation of the adaptor proteins, such as Gab1, Grb2, and Src, which then blocks the Raf1/ERK signaling (32). Therefore, LECT2 plays a suppressive role in vascular invasion and metastasis in HCC by acting as a ligand for c-Met but not as an endopeptidase. Interestingly, similarly to LECT2, the β-chain of hepatocyte growth factor, a cognate ligand of c-Met, has a chymotrypsin-like serine protease fold but lacks the hydrolytic activity due to the absence of certain catalytic residues (35). The complex structure reveals that hepatocyte growth factor β binds to c-Met by utilizing its pseudo-active site region (35).

In addition to LECT2, other noncatalytic bacterial proteins with an M23 metalloendopeptidase fold have been found to engage in protein-protein interactions. For example, the extracellular LytM-like domain of the forespore-expressed membrane protein SpoIIQ from *Bacillus subtilis* has no metalloendopeptidase activity because it lacks certain active site residues and a catalytic metal ion. In addition, the substrate-binding groove is closed off by its additional N-terminal β-hairpin region. However, SpoIIQ has developed a novel function for mediating protein-protein interactions that are specifically mediated by this additional region (36, 37). Another example is the *Escherichia coli* cell division protein EnvC. Although the C-terminal LytM domain of EnvC also lacks conserved Zn(II)-coordinating and catalytic residues and is not capable of functioning as a metalloendopeptidase, it can activate amidases that can hydrolyze peptidoglycan. A mutational analysis and molecular modeling studies have suggested that EnvC might use the catalytically inactive groove to bind the amidase autoinhibitory α-helix (38, 39). Based on the examples of SpoIIQ and EnvC, we suspect that the nonconserved N-terminal IC loop together with the central groove of LECT2 may be specific for interactions between LECT2 and its partners. Interestingly, some mul-

tiple domain proteins of the M23 family adopt an autoinhibited state as the result of interactions between two domains. This observation suggests possible binding modes for the protein-protein interactions that occur in those noncatalytic homologs. For instance, in the structure of full-length LytM, a loop from the N-terminal domain binds within the active site groove of the C-terminal catalytic domain, and an asparagine residue on this inhibitory loop occupies one of the ligand sites of Zn(II) (25). Another example is the structure of NMB0315 from *Neisseria meningitides*. The N-terminal short $\beta3$-$\beta4$ loop stretches into the active site groove of the C-terminal catalytic domain but is not involved in the Zn(II) coordination (40). These inhibitory segments do not fit into the active site such as a substrate but occupy the substrate-binding groove by tight interactions.

Our study of the structure of LECT2 combined with the findings for other noncatalytic proteins with an M23 metalloendopeptidase fold that we discussed above reveals that these proteins share some common features. Specifically, they lack residues that are important for peptidase activity and/or show variations in the N-terminal region. These variations suggest an efficient mechanism for the evolution of new functions. Although our data do not exclude the possibility that LECT2 has a peptidase activity against a specific peptide sequence, human LECT2 has evolved from a catalytically competent ancestor to a receptor-binding protein that is involved in an important signaling pathway. This function may require the peptidase-inhibitor binding mode for the protein-protein interactions.

Experimental Procedures

Protein Preparation—The human LECT2 was expressed and purified as described previously (41, 42). Briefly, a DNA sequence encoding the mature human LECT2 was amplified by PCR and cloned into the SmaI/BamHI site of the pET-48b(+) expression plasmid (Novagen). LECT2 with the N-terminal thioredoxin-hexahistidine (His_6) tag was overexpressed in *E. coli* strain Rosetta-gami 2 (DE3) (Novagen). The structure determination was performed using selenomethionine-substituted LECT2 ($LECT2^{SeMet}$) that was produced in M9 medium containing various amino acids (100 mg/liter L-lysine, L-phenylalanine, and L-threonine and 50 mg/liter L-isoleucine, L-leucine, L-valine, and L-selenomethionine). After expression of the protein, the harvested cells were disrupted by sonication, and centrifugation was used to separate the insoluble inclusion bodies from the soluble proteins. The suspension of LECT2 inclusion bodies was adjusted to a protein concentration of 0.5 mg/ml in the refolding buffer (50 mM Tris-HCl (pH 8.0) and 500 mM L-arginine) and subjected to high hydrostatic pressure (200 megapascals) in a PreEMT-E150 pressure chamber (BaroFold Inc.) overnight at room temperature. The solution containing the refolded LECT2 was dialyzed to remove L-arginine before purification. The expressed soluble LECT2 and the refolded protein were separately applied to a nickel-nitrilotriacetic acid Superflow (Qiagen) column. The protein was released by addition of HRV3C protease to the column to remove the N-terminal tag, and the eluted protein was further purified using cation exchange chromatography on a Resource S column (GE Healthcare).

Crystallization and X-ray Data Collection—The refolded $LECT2^{SeMet}$ was concentrated to 10 mg/ml in a final buffer containing 10 mM Tris-HCl (pH 7.0), 1 mM iminodiacetic acid, and 50 μM $ZnCl_2$ and was then crystallized using the sitting drop vapor diffusion method (42). The best crystals were obtained by mixing 1.0 μl of the protein solution with 1.0 μl of the reservoir solution, which consisted of 0.2 M ammonium sulfate, 0.1 M HEPES (pH 7.5), and 25% (w/v) PEG 8000 at 20 °C. The x-ray diffraction data were collected using the BL-5A beamline at the Photon Factory (Tsukuba, Japan) with an ADSC Quantum 210r CCD detector. A crystal of $LECT2^{SeMet}$ was used to collect a single wavelength anomalous dispersion data set at the selenium peak wavelength of 0.9792 Å. The data set was indexed and integrated using the HKL2000 program suite (43). Table 1 summarizes the data collection and data processing statistics.

Structure Determination and Refinement—The selenium positions in the protein crystal were determined with SHELXD (44). Heavy atom refinement and phase calculations were performed with SHARP (45). An initial model was automatically built with the ARP/wARP package from the CCP4 suite (46). The missing amino acid residues were manually added using Coot (47). The obtained model was refined using Refmac5 (48) from the CCP4 program suite. Iterative rounds of refinements were continued with Coot and Refmac5. The crystallographic water molecules were automatically introduced using ARP/wARP with subsequent manual modification. The quality of the model was verified using PROCHECK (49). The final crystal structure was refined to R_{work} and R_{free} values of 17.7 and 22.3%, respectively. The refinement statistics are summarized in Table 1. The visualization and superimposition of the protein structures were achieved using PyMOL, and the r.m.s.d. values for superimposed structures were calculated using the Dali server (50).

Site-directed Mutagenesis—The LECT2 Y86H mutant was generated with the PCR-based site-directed mutagenesis method using a QuikChange site-directed mutagenesis kit (Stratagene) (51) with the pET48b-LECT2 plasmid as a template. The primers were purchased from Operon Technologies Inc. and designed as follows: 5′-GGAAGAGGTTTTTGTGTCAAAATGTTCCACATTAAGCCAATTAAG-3′ and 5′-CTTAATT GGCTTAATGTGGAACATTTTGACACAAAAACCTCTTCC-3′. The underlined characters in the primer sequences are the altered nucleobases. The mutation was verified by the DNA sequencing service of FASMAC. The Y86H mutant was expressed in soluble form and purified according to the method described for the wild-type LECT2.

M23 Metalloendopeptidase Activity Assay—The assay was performed according to a previous report with some modifications (25, 26). The soluble form of the expressed LECT2 was concentrated to 5 mg/ml in a buffer containing 10 mM Tris-HCl (pH 7.0) and 50 μM $ZnCl_2$. Subsequently, 0.2 mg/ml LECT2 or lysostaphin was incubated with 1 mM pentaglycine as the substrate (Bachem AG) for 24 h at 37 °C in 20 mM Tris-HCl (pH 7.5) with a final Zn(II) concentration of 2 μM. The mature recombinant lysostaphin from *Staphylococcus simulans* biovar *staphylolyticus* (Wako) was used as a positive control in the assay system. After the reaction, the enzyme activity was mea-

TABLE 1

Data collection and refinement statistics

The values in parentheses are for the highest resolution shell. r.m.s.d., root mean square deviation.

	$LECT2^{SeMet}$-Zn(II)
Data collection	
Beamline	PF BL-5A
Wavelength (Å)	0.9792
Space group	$P2_12_12_1$
Unit cell parameters (Å)	$a = 59.4$, $b = 63.5$, $c = 64.0$
Resolution range (Å)	50.0–1.94 (2.01–1.94)
No. of unique reflections	18,525 (1,764)
Redundancy	14.1 (11.5)
Completeness (%)	99.7 (97.2)
R_{sym}[a]	0.072 (0.224)
R_{pim}[b]	0.024 (0.068)
$I/\sigma(I)$	51.9 (12.8)
Refinement	
Resolution (Å)	47.1–1.94 (2.01–1.94)
No. reflections	18,479
R_{work}/R_{free} (%)[c]	17.7/22.3
No. atoms	
Protein	2,044
Zn(II)	2
Water	167
Average B-factors (Å^2)	
Protein	17.5
Zn(II)	11.8
Water	26.3
r.m.s.d.	
Bond lengths (Å)	0.019
Bond angles (°)	1.745
Ramachandran plot	
Favored, allowed, disallowed (%)	95.04, 3.82, 1.15

[a] $R_{sym} = \Sigma_{hkl}\Sigma_i|I_i(hkl) - \langle I(hkl)\rangle|/\Sigma_{hkl}\Sigma_i I_i(hkl)$ where $I_i(hkl)$ and $\langle I(hkl)\rangle$ are the observed intensity and average intensity of multiple observations from symmetry-related reflections, respectively.

[b] $R_{pim} = \Sigma_{hkl}\{1/[N(hkl) - 1]\}^{1/2} \times \Sigma_i|I_i(hkl) - \langle I(hkl)\rangle|/\Sigma_{hkl}\Sigma_i I_i(hkl)$ where $N(hkl)$ is the redundancy, $I_i(hkl)$ is the observed intensity, and $\langle I(hkl)\rangle$ is the average intensity of multiple observations from symmetry-related reflection.

[c] R_{work} was calculated with 95% of the data used for refinement, and R_{free} was calculated with 5% of the data excluded from refinement.

sured using TLC. Samples of 2 μl of the reaction mixture were applied to a TLC plate covered by Silica Gel 60 (Merck), and the plate was dried and developed in a chamber pre-equilibrated with the mobile phase solvent (*n*-butyl alcohol/acetic acid/water; 4:1:1 by volume). To visualize the spots, the plate was sprayed with ninhydrin solution and heated to 100 °C.

Endopeptidase Activity Assay—The endopeptidase activity of LECT2 was assayed against various types of proteins. Casein was used as a generic proteinase substrate because it is digested by a wide range of proteinases. Azocasein (Sigma) was purified by Q-Sepharose Fast Flow (GE Healthcare), and the purity of azocasein was evaluated using SDS-PAGE. A broad range standard protein mixture (Bio-Rad) that contained nine different proteins was also used as a substrate. Before use in the assay, the purified LECT2 was diluted with 10 mM Tris-HCl (pH 7.0) and 5 μM $ZnCl_2$ to permit Zn(II) uptake. The protein was then concentrated to >300 μM by ultrafiltration. Azocasein or the standard protein mixture was incubated with LECT2 (1–5 μM) for 24 h at 37 °C in 20 mM Tris-HCl (pH 7.5) with 1 μM $ZnCl_2$. After the reaction, the samples were evaluated using SDS-PAGE.

Surface Plasmon Resonance Analysis—The interaction of LECT2 with the c-Met receptor was measured using surface plasmon resonance with a Biacore T200 instrument equipped with a Series S sensor chip SA (GE Healthcare) at 25 °C. This chip contains preimmobilized streptavidin and is used for high affinity capture of biotinylated ligands. Therefore, the recombinant human c-Met ECD (Glu^{25}–Thr^{932}; Sino Biological Inc.) was first biotinylated by incubation with an equimolar amount of sulfo-NHS-LC-LC-biotin (Pierce) on ice for 2 h after which the unreacted biotin was removed using size exclusion chromatography on a Superdex 200 HR 10/30 column (GE Healthcare). A total of 1963 response units of the biotinylated c-Met ECD were immobilized on the flow cell of the SA sensor chip. The remaining binding sites were blocked with 1 μM free biotin to reduce the nonspecific binding of protein. For the kinetic measurements, LECT2 at concentrations ranging from 0.125 to 8 μM in the running buffer (10 mM HEPES (pH 7.4), 150 mM NaCl, 50 μM $ZnCl_2$, and 0.005% Tween 20) was injected over the c-Met surface and the blank flow cell for 2 min at a flow rate of 30 μl/min, and then the bound LECT2 was allowed to dissociate for 10 min. Finally, the resulting data were analyzed with the Biacore T200 evaluation software using a steady-state affinity model.

Author Contributions—M. T. designed the study. H. Z. and A. A. performed the experiments. H. Z. and T. M. collected and analyzed the x-ray diffraction data. H. Z., T. M., and M. T. wrote the paper. Y. S., A. O., and S. Y. provided technical assistance. M. T. supervised the entire project. All authors have approved the final version of the manuscript.

Acknowledgments—We thank the scientists and staff at the Photon Factory, Tsukuba, Japan. The synchrotron radiation experiments were performed on the BL-5A beamline at the Photon Factory (Proposal Number 2008S2–001). We also thank Prof. Kazuo Suzuki (Teikyo University) for critical discussions.

References

1. Yamagoe, S., Yamakawa, Y., Matsuo, Y., Minowada, J., Mizuno, S., and Suzuki, K. (1996) Purification and primary amino acid sequence of a novel neutrophil chemotactic factor LECT2. *Immunol. Lett.* **52,** 9–13
2. Yamagoe, S., Mizuno, S., and Suzuki, K. (1998) Molecular cloning of human and bovine LECT2 having a neutrophil chemotactic activity and its specific expression in the liver. *Biochim. Biophys. Acta* **1396,** 105–113
3. Segawa, Y., Itokazu, Y., Inoue, N., Saito, T., and Suzuki, K. (2001) Possible changes in expression of chemotaxin LECT2 mRNA in mouse liver after concanavalin A-induced hepatic injury. *Biol. Pharm. Bull.* **24,** 425–428
4. Ovejero, C., Cavard, C., Périanin, A., Hakvoort, T., Vermeulen, J., Godard, C., Fabre, M., Chafey, P., Suzuki, K., Romagnolo, B., Yamagoe, S., and Perret, C. (2004) Identification of the leukocyte cell-derived chemotaxin 2 as a direct target gene of β-catenin in the liver. *Hepatology* **40,** 167–176
5. Phesse, T. J., Parry, L., Reed, K. R., Ewan, K. B., Dale, T. C., Sansom, O. J., and Clarke, A. R. (2008) Deficiency of Mbd2 attenuates Wnt signaling. *Mol. Cell. Biol.* **28,** 6094–6103
6. Liu, H., Fergusson, M. M., Wu, J. J., Rovira, I. I., Liu, J., Gavrilova, O., Lu, T., Bao, J., Han, D., Sack, M. N., and Finkel, T. (2011) Wnt signaling regulates hepatic metabolism. *Sci. Signal.* **4,** ra6
7. Saito, T., Okumura, A., Watanabe, H., Asano, M., Ishida-Okawara, A., Sakagami, J., Sudo, K., Hatano-Yokoe, Y., Bezbradica, J. S., Joyce, S., Abo, T., Iwakura, Y., Suzuki, K., and Yamagoe, S. (2004) Increase in hepatic NKT cells in leukocyte cell-derived chemotaxin 2-deficient mice contributes to severe concanavalin A-induced hepatitis. *J. Immunol.* **173,** 579–585
8. Okumura, A., Saito, T., Otani, I., Kojima, K., Yamada, Y., Ishida-Okawara, A., Nakazato, K., Asano, M., Kanayama, K., Iwakura, Y., Suzuki, K., and Yamagoe, S. (2008) Suppressive role of leukocyte cell-derived chemotaxin

2 in mouse anti-type II collagen antibody-induced arthritis. *Arthritis Rheum.* **58,** 413–421
9. Kameoka, Y., Yamagoe, S., Hatano, Y., Kasama, T., and Suzuki, K. (2000) Val58Ile polymorphism of the neutrophil chemoattractant LECT2 and rheumatoid arthritis in the Japanese population. *Arthritis Rheum.* **43,** 1419–1420
10. Graessler, J., Verlohren, M., Graessler, A., Zeissig, A., Kuhlisch, E., Kopprasch, S., and Schroeder, H. E. (2005) Association of chondromodulin-II Val58Ile polymorphism with radiographic joint destruction in rheumatoid arthritis. *J. Rheumatol.* **32,** 1654–1661
11. Ong, H. T., Tan, P. K., Wang, S. M., Hian Low, D. T., Ooi, L. L., and Hui, K. M. (2011) The tumor suppressor function of LECT2 in human hepatocellular carcinoma makes it a potential therapeutic target. *Cancer Gene Ther.* **18,** 399–406
12. Anson, M., Crain-Denoyelle, A. M., Baud, V., Chereau, F., Gougelet, A., Terris, B., Yamagoe, S., Colnot, S., Viguier, M., Perret, C., and Couty, J. P. (2012) Oncogenic β-catenin triggers an inflammatory response that determines the aggressiveness of hepatocellularcarcinoma in mice. *J. Clin. Investig.* **122,** 586–599
13. Okumura, A., Unoki-Kubota, H., Matsushita, Y., Shiga, T., Moriyoshi, Y., Yamagoe, S., and Kaburagi, Y. (2013) Increased serum leukocyte cell-derived chemotaxin 2 (LECT2) levels in obesity and fatty liver. *Biosci. Trends* **7,** 276–283
14. Lan, F., Misu, H., Chikamoto, K., Takayama, H., Kikuchi, A., Mohri, K., Takata, N., Hayashi, H., Matsuzawa-Nagata, N., Takeshita, Y., Noda, H., Matsumoto, Y., Ota, T., Nagano, T., Nakagen, M., *et al.* (2014) LECT2 functions as a hepatokine that links obesity to skeletal muscle insulin resistance. *Diabetes* **63,** 1649–1664
15. Murphy, C. L., Wang, S., Kestler, D., Larsen, C., Benson, D., Weiss, D. T., and Solomon, A. (2010) Leukocyte chemotactic factor 2 (LECT2)-associated renal amyloidosis: a case series. *Am. J. Kidney Dis.* **56,** 1100–1107
16. Mereuta, O. M., Theis, J. D., Vrana, J. A., Law, M. E., Grogg, K. L., Dasari, S., Chandan, V. S., Wu, T. T., Jimenez-Zepeda, V. H., Fonseca, R., Dispenzieri, A., Kurtin, P. J., and Dogan, A. (2014) Leukocyte cell-derived chemotaxin 2 (LECT2)-associated amyloidosis is a frequent cause of hepatic amyloidosis in the United States. *Blood* **123,** 1479–1482
17. Kowalski, A., Cabrera, J., Nasr, S., and Lerma, E. (2015) Renal LECT2 amyloidosis: a newly described disorder gaining greater recognition. *Clin. Nephrol.* **84,** 236–240
18. Okumura, A., Suzuki, T., Dohmae, N., Okabe, T., Hashimoto, Y., Nakazato, K., Ohno, H., Miyazaki, Y., and Yamagoe, S. (2009) Identification and assignment of three disulfide bonds in mammalian leukocyte cell-derived chemotaxin 2 by matrix-assisted laser desorption/ionization time-of-flight mass spectrometry. *Biosci. Trends* **3,** 139–143
19. Finn, R. D., Bateman, A., Clements, J., Coggill, P., Eberhardt, R. Y., Eddy, S. R., Heger, A., Hetherington, K., Holm, L., Mistry, J., Sonnhammer, E. L., Tate, J., and Punta, M. (2014) Pfam: the protein families database. *Nucleic Acids Res.* **42,** D222–D230
20. Sugai, M., Fujiwara, T., Akiyama, T., Ohara, M., Komatsuzawa, H., Inoue, S., and Suginaka, H. (1997) Purification and molecular characterization of glycylglycine endopeptidase produced by *Staphylococcus capitis* EPK1. *J. Bacteriol.* **179,** 1193–1202
21. Ramadurai, L., Lockwood, K. J., Nadakavukaren, M. J., and Jayaswal, R. K. (1999) Characterization of a chromosomally encoded glycylglycine endopeptidase of *Staphylococcus aureus*. *Microbiology* **145,** 801–808
22. Park, P. W., and Mecham, R. P. (2004) *Handbook of Proteolytic Enzymes* (Barrett, A. J., Rawlings, N. D., and Woessner, J. F., eds) 2nd Ed., pp. 1004–1005, Elsevier, London
23. Firczuk, M., and Bochtler, M. (2007) Folds and activities of peptidoglycan amidases. *FEMS Microbiol. Rev.* **31,** 676–691
24. Spencer, J., Murphy, L. M., Conners, R., Sessions, R. B., and Gamblin, S. J. (2010) Crystal structure of the LasA virulence factor from *Pseudomonas aeruginosa*: substrate specificity and mechanism of M23 metallopeptidases. *J. Mol. Biol.* **396,** 908–923
25. Odintsov, S. G., Sabala, I., Marcyjaniak, M., and Bochtler, M. (2004) Latent LytM at 1.3 Å resolution. *J. Mol. Biol.* **335,** 775–785
26. Firczuk, M., Mucha, A., and Bochtler, M. (2005) Crystal structures of active LytM. *J. Mol. Biol.* **354,** 578–590
27. Ragumani, S., Kumaran, D., Burley, S. K., and Swaminathan, S. (2008) Crystal structure of a putative lysostaphin peptidase from *Vibrio cholerae*. *Proteins* **72,** 1096–1103
28. Sabala, I., Jagielska, E., Bardelang, P. T., Czapinska, H., Dahms, S. O., Sharpe, J. A., James, R., Than, M. E., Thomas, N. R., and Bochtler, M. (2014) Crystal structure of the antimicrobial peptidase lysostaphin from *Staphylococcus simulans*. *FEBS J.* **281,** 4112–4122
29. Cohen, D. N., Sham, Y. Y., Haugstad, G. D., Xiang, Y., Rossmann, M. G., Anderson, D. L., and Popham, D. L. (2009) Shared catalysis in virus entry and bacterial cell wall depolymerization. *J. Mol. Biol.* **387,** 607–618
30. Xiang, Y., Morais, M. C., Cohen, D. N., Bowman, V. D., Anderson, D. L., and Rossmann, M. G. (2008) Crystal and cryoEM structural studies of a cell wall degrading enzyme in the bacteriophage ϕ29 tail. *Proc. Natl. Acad. Sci. U.S.A.* **105,** 9552–9557
31. Singh, S. K., SaiSree, L., Amrutha, R. N., and Reddy, M. (2012) Three redundant murein endopeptidases catalyse an essential cleavage step in peptidoglycan synthesis of *Escherichia coli* K12. *Mol. Microbiol.* **86,** 1036–1051
32. Chen, C. K., Yang, C. Y., Hua, K. T., Hua, K. T., Ho, M. C., Johansson, G., Jeng, Y. M., Chen, C. N., Chen, M. W., Lee, W. J., Su, J. L., Lai, T. C., Chou, C. C., Ho, B. C., Chang, C. F., *et al.* (2014) Leukocyte cell-derived chemotaxin 2 antagonizes MET receptor activation to suppress hepatocellular carcinoma vascular invasion by protein tyrosine phosphatase 1B recruitment. *Hepatology* **59,** 974–985
33. Vessillier, S., Delolme, F., Bernillon, J., Saulnier, J., and Wallach, J. (2001) Hydrolysis of glycine-containing elastin pentapeptides by LasA, a metalloelastase from *Pseudomonas aeruginosa*. *Eur. J. Biochem.* **268,** 1049–1057
34. Alberts, I. L., Nadassy, K., and Wodak, S. J. (1998) Analysis of zinc binding sites in protein crystal structures. *Protein Sci.* **7,** 1700–1716
35. Kirchhofer, D., Yao, X., Peek, M., Eigenbrot, C., Lipari, M. T., Billeci, K. L., Maun, H. R., Moran, P., Santell, L., Wiesmann, C., and Lazarus, R. A. (2004) Structural and functional basis of the serine protease-like hepatocyte growth factor β-chain in Met binding and signaling. *J. Biol. Chem.* **279,** 39915–39924
36. Levdikov, V. M., Blagova, E. V., McFeat, A., Fogg, M. J., Wilson, K. S., and Wilkinson, A. J. (2012) Structure of components of an intercellular channel complex in sporulating *Bacillus subtilis*. *Proc. Natl. Acad. Sci. U.S.A.* **109,** 5441–5445
37. Meisner, J., Maehigashi, T., André, I., Dunham, C. M., and Moran, C. P., Jr. (2012) Structure of the basal components of a bacterial transporter. *Proc. Natl. Acad. Sci. U.S.A.* **109,** 5446–5451
38. Uehara, T., Parzych, K. R., Dinh, T., and Bernhardt, T. G. (2010) Daughter cell separation is controlled by cytokinetic ring-activated cell wall hydrolysis. *EMBO J.* **29,** 1412–1422
39. Peters, N. T., Morlot, C., Yang, D. C., Uehara, T., Vernet, T., and Bernhardt, T. G. (2013) Structure-function analysis of the LytM domain of EnvC, an activator of cell wall remodelling at the *Escherichia coli* division site. *Mol. Microbiol.* **89,** 690–701
40. Wang, X., Yang, X., Yang, C., Wu, Z., Xu, H., and Shen, Y. (2011) Crystal structure of outer membrane protein NMB0315 from *Neisseria meningitides*. *PLoS One* **6,** e26845
41. Zheng, H., Miyakawa, T., Sawano, Y., Yamagoe, S., and Tanokura, M. (2013) Expression, high-pressure refolding and purification of human leukocyte cell-derived chemotaxin 2 (LECT2). *Protein Expr. Purif.* **88,** 221–229
42. Zheng, H., Miyakawa, T., Sawano, Y., Yamagoe, S., and Tanokura, M. (2013) Crystallization and preliminary x-ray analysis of human leukocyte cell-derived chemotaxin 2 (LECT2). *Acta Crystallogr. Sect. F Struct. Biol. Cryst. Commun.* **69,** 316–319
43. Otwinowski, Z., and Minor, W. (1997) Processing of x-ray diffraction data collected in oscillation mode. *Methods Enzymol.* **276,** 307–326
44. Schneider, T. R., and Sheldrick, G. M. (2002) Substructure solution with SHELXD. *Acta Crystallogr. D Biol. Crystallogr.* **58,** 1772–1779
45. La Fortelle, E., and de Bricogne, G. (1997) Maximum likelihood heavy-atom parameter refinement for multiple isomorphous replacement and multiwavelength anomalous diffraction methods. *Methods Enzymol.* **276,** 472–494

46. Perrakis, A., Harkiolaki, M., Wilson, K. S., and Lamzin, V. S. (2001) ARP/wARP and molecular replacement. *Acta Crystallogr. D Biol. Crystallogr.* **57,** 1445–1450
47. Emsley, P., and Cowtan, K. (2004) Coot: model-building tools for molecular graphics. *Acta Crystallogr. D Biol. Crystallogr.* **60,** 2126–2132
48. Murshudov, G. N., Vagin, A. A., and Dodson, E. J. (1997) Refinement of macromolecular structures by the maximum-likelihood method. *Acta Crystallogr. D Biol. Crystallogr.* **53,** 240–255
49. Laskowski, R. A., MacArthur, M. W., Moss, D. S., and Thorntonan, J. M. (1993) PROCHECK: a program to check the stereochemical quality of protein structures. *J. Appl. Crystallogr.* **26,** 283–291
50. Holm, L., and Rosenström, P. (2010) Dali server: conservation mapping in 3D. *Nucleic Acids Res.* **38,** W545–W549
51. Papworth, C., Bauer, J. C., Braman, J., and Wright, D. A. (1996) Site-directed mutagenesis is one day with >80% efficiency. *Strategies* **9,** 3–4